EUROPEAN ORGANIZATION FOR NUCLEAR RESEARCH

CERN-PPE/91-135
12.8.1991

RESONANCE IONIZATION SPECTROSCOPY ON A FAST ATOMIC YTTERBIUM BEAM*

Ch. Schulz, E. Arnold, W. Borchers, W. Neu, R. Neugart, M. Neuroth,
E.W. Otten, M. Scherf, K. Wendt,
Institut für Physik, Universität Mainz, Mainz, Germany

P. Lievens*,
Instituut voor Kern- en Stralingsfysika, K.U. Leuven, Leuven, Belgium

Yu.A. Kudryavtsev, V.S. Letokhov, V.I. Mishin, V.V. Petrunin,
Institute of Spectroscopy, USSR Academy of Sciences, Troitzk, USSR

and the ISOLDE Collaboration, PPE Div., CERN, Geneva, Switzerland

ABSTRACT

Resonance ionization spectroscopy in collinear geometry has been successfully applied to a fast beam of ytterbium atoms. The atoms were excited stepwise into a Rydberg state by pulsed last light, ionized in an electrical field and deflected onto a secondary electron detector. The efficiency was 1.10^{-5} detected ions per incoming atom on a background from collisional ionization of 1.10^{-8}. The technique has been exploited for the measurement of hyperfine structures and isotope shifts of unstable ytterbium isotopes, in particular ^{187}Yb, ^{159}Yb and ^{175}Yb.

Submitted to J. Phys. B.

(IS82)

---

*) Present address: PPE Division, CERN, Geneva, Switzerland
PACS numbers: 31.30.G 35.10.F 32.80.K 27.70
Short title: RIS on a Fast Atomic Beam

1 Introduction

Laser spectroscopy has been used extensively for the investigation of nuclear moments and radii of unstable isotopes. Special attention has been paid to a systematic study of the rare earth region, where on-line mass separators deliver beams of up to 20 neutron deficient isotopes of many elements (Ravn et al. 1988). Two different techniques have provided most of the present results in this region: collinear laser spectroscopy on fast beams (Neugart 1987) and resonance ionization spectroscopy (RIS) on thermal atomic beams (Balykin et al. 1980, Alkhazov et al. 1988). Comparing these two methods, one finds that the main advantage of the RIS scheme consists in *(i)* an efficient detection of the ions produced by laser excitation and *(ii)* a high selectivity and background supression due to several consecutive excitation steps. A drawback of the method is the incomplete spatial, spectral and temporal overlap between the atomic absorption profile and the spectrum of the pulsed laser (Ruster et al. 1989). Collinear laser fluorescence spectroscopy offers the advantages of continuous excitation and a complete spectral overlap due to the reduction of the Doppler width by the electrostatic acceleration (Kaufmann 1976). On the other hand, this technique has to cope with a higher background from stray-light, radioactivity and photons from the decay of long-lived states populated in the neutralization cell. Both the signal and the background are higher than for the RIS scheme, but the practical sensitivity limit of $10^5 - 10^7\ atoms/sec$ is approximately the same.

A combination of both techniques for experiments on rare earth isotopes with very low production yields was proposed by Letokhov and Mishin (1984). This scheme preserves the excitation efficiency at high resolution achieved in collinear geometry and takes advantage of the efficient detection and background suppression of resonance ionization. It promises a considerable improvement in sensitivity, although the use of a pulsed laser with a continuous beam involves duty cycle losses. The high selectivity of RIS in a fast beam (Kudryavtsev and Letokhov 1982) has also been exploited for the trace analysis of ^3He (Aseyev et al. 1991). The present paper reports on an application of this scheme to the study of radioactive ytterbium isotopes produced at very low rates. Ytterbium offers a simple spectrum and the io-

nization limit can be reached with only two excitation steps from metastable states. Direct comparisons are possible with other techniques using collinear excitation and fluorescence detection (Buchinger et al. 1982, Neugart et al. 1983) and fluorescence spectroscopy in a cooled buffer gas cell (Sprouse et al. 1989).

2 Resonance ionization spectroscopy on ytterbium

The principle of RIS is as follows: The atoms are excited into an autoionizing state or into a Rydberg state from which they can be ionized by an electrical field with a modest field strength. The ions are then counted by a secondary electron multiplier. Maximum ionization efficiency is reached if *(i)* all transitions are saturated and *(ii)* optical pumping into states outside the RIS ladder is minimized. Both conditions require the high power of pulsed dye lasers with a pulse duration shorter than (or at least comparable to) the lifetimes of the states involved. The bandwidth of these lasers, $5\,GHz < \delta\nu < 30\,GHz$, is larger than the typical hyperfine structures and thus enables the simultaneous excitation of all sublevels. On the other hand, narrow band excitation in one of the excitation steps is required for the resolution of hyperfine splittings which yield the information about nuclear moments. This is achieved using pulsed amplification of cw dye laser radiation with a Fourier-limited bandwidth of $\Delta\nu \approx 50MHz$ (Lavi et al. 1986).

Fig. 1 shows part of the energy levels in the $Yb\,I$ spectrum. As the initial state of the RIS ladder we chose the metastable $6s6p\,^3P_0$ which is populated in the charge - exchange neutralization process applied to the $60\,keV$ ions. From this state, the atoms are excited via $6s7s\,^3S_1$ ($\lambda_1 = 648.9nm$) into one of the $6s21p\,^3P_{0,1,2}, {}^1P_0$ ($\lambda_2 = 575.6nm$) Rydberg states from which the ionization takes place. The field strength necessary for ionization of these Rydberg atoms can be calculated roughly by the classical formula (Ducas et al. 1975)

$$|F| \approx 3 \times 10^{10} \frac{1}{n^{*4}} \frac{V}{m}, \qquad (1)$$

where $n^* \approx n - 4 = 17$ (Bekov et al. 1980) is the effective quantum number. This yields $|F| \approx 4 \cdot 10^5 \frac{V}{m}$.

In this excitation scheme, the optical pumping losses are mainly due to the

decay of the intermediate $6s7s\,^3S_1$ state into the states $6s6p\,^3P_2,^3P_1$ ($\tau_2 \approx 20nsec$). The Rydberg states have a lifetime of $\tau_3 \approx 5\mu sec$ which is somewhat larger than the time of flight through the interaction region. With the laser pulse satisfying the condition $\tau_L < 1/(2\Gamma_p)$, Γ_p beeing the partial decay width of the excited state, the flux of photons per laser pulse necessary for saturation, Q_{SAT}, can be estimated from the relation

$$\sigma_E Q_{SAT} \geq 1/2.$$

The saturation cross section σ_e is given by:

$$\sigma_E = \frac{\lambda^2}{2\pi} \times \frac{\Gamma_p}{\Gamma_t} \times \frac{1}{\sqrt{\pi}\Delta\nu_D} \int_{-\infty}^{\infty} \frac{exp(-(\nu' - \nu_0)^2/\Delta\nu_D^2)}{1 + (4\pi(\nu - \nu')/\Gamma_t)^2}\, d\nu', \tag{2}$$

where λ is the transition wavelength and Γ_p/Γ_t the ratio between the partial and the total decay width (Otten 1988). The integral containing the Doppler width $\Delta\nu_D$ describes the normalized lineshape of the transition. If the laser bandwidth $\Delta\nu_L$ exceeds the homogenous absorption width $\Delta\nu_H$, Q_{SAT} is additionally increased by a factor $\Delta\nu_L/\Delta\nu_H$ (Ruster et al. 1989),

$$Q_{SAT} \geq \frac{\Delta\nu_L}{\Delta\nu_H} \frac{1}{2\sigma_E}. \tag{3}$$

The dependency of the saturation power on the ratio $(\Delta\nu_L/\Delta\nu_H)$ makes it most favourable to take the weak transition into the Rydberg state ($\Delta\nu_H < 30\,kHz$) as the high resolution step. The amplified cw laser gives a maximum spectral density over the small homogenous linewidth. Under these conditions, saturation in the first step should be reached at an average laser power of $P_L \approx 20mW$ (repetition rate: $10\,kHz$, pulse energy: $2\,\mu J/pulse$ at $\Delta\nu_{Laser} \approx 30GHz$). The saturation power for the second transition is 50 times higher because of the small spectral overlap.

For a short laser pulse, the maximum excitation efficiency ϵ_{exc} from the metastable state to the Rydberg state is given by the statistical weights of the states involved,

$$\epsilon_{exc} \leq \frac{2J_f + 1}{1 + 3 + 2J_f + 1}, \tag{4}$$

which yields values between 20% and 62% for different angular momenta J_f of the final state, $0 < J_f < 2$ (see below). With the exciting pulse duration amounting to some $18\,ns$, the quantity ϵ_{exc} decreases by a factor of 2 as a result of the decay of

the intermediate state $6s7s\,^3S_1$. For incomplete saturation it decreases by another factor P_L/P_{SAT}, the ratio of the laser power to the saturation power.

The upper excitation step can lead to one of the four fine structure (FS) components of the $6s\,21p$ Rydberg state. Of these, the $^3P_2$ state has the highest statistical weight. As can be seen from Fig.1, the FS splitting between the $6s21p\,^3P_2$ and the $6s21p\,^1P_1$ states is only 6.25 GHz (see section 4). The hyperfine structure (HFS) in both these states is dominated by the interaction of the $6s$ electron with the nucleus ($a_{6s} \approx 3.5\,GHz$ for ^{173}Yb (Münch et al. 1987)), so that the HFS splittings of both states partially overlap. In this situation the FS and the HFS have to be treated by a common diagonalization of the interaction matrix, which complicates the analysis of the data considerably. The choice of a transition to the $^3P_1$ state has the advantage that the nearest neighbour $^3P_2$ is $104\,GHz$ away. Here the analysis of the data still requires second order perturbation theory for the treatment of the HFS. The measurements have partly been performed in the transitions to both FS states, $^3P_2$ and $^3P_1$, in order to check the consistency of the analyses.

3 Experimental setup

The experiment has been carried out at the ISOLDE isotope separator facility at CERN. The unstable ytterbium isotopes are produced in the spallation reactions $^{181}Ta(p, 4p + xn)^{178-x}Yb$. They are ionized, accelerated to $60\,keV$ and separated in a magnet. The fast ion beam is then superimposed on the merged laser beams. The experimental setup is shown in Fig. 2. The ion beam passes through the neutralization cell, where the metastable $6s6p\ ^3P_0$ state is populated, along with other states, in quasi-resonant charge exchange collisions with caesium atoms. At the exit of the charge exchange cell, the remaining ions and the atoms in highly excited Rydberg states ($n \geq 20$), are filtered from the beam by the electrical field ($5 \cdot 10^5 V/m$) of a capacitor (Filter 1). The beam then enters the excitation region ($l = 100cm$), where the metastable atoms in the $6s6p\,^3P_0$ state undergo the two-step excitation to one of the $6s21p$ Rydberg states. The Rydberg atoms are ionized in the electrical field of the ionizer ($E_i = 4 \cdot 10^5\ V/m$) and deflected to the detector. Tuning of the effective laser frequency seen by the neutral atoms is accomplished by

applying a variable potential to the charge exchange cell (Doppler-tuning). Then the voltage at the last deflector has to be varied synchronously with the Doppler-tuning voltage.

A laser with a large bandwidth of $\Delta\nu_{L1} = 30GHz$ is used to excite the atoms in the first step ($\lambda_1 = 648.9\,nm$). The average output power of this laser ($150\,mW$) is enough to saturate the first transition. The second-step radiation ($\lambda_2 = 575.6\,nm$) is obtained by amplifying the output of a single-frequency cw ring laser (Coherent CR 699/21) in a cell containing the dye Rhodamin 6G. The average amplified output power is $0.5\,W$ and the bandwidth $\Delta\nu_{L2} \approx 50\,MHz$, corresponding to the Fourier transform of the pulse shape. The broad band laser and the amplification cell are pumped with a $10\,W$ copper vapour laser (CVL) in a master oscillator - amplifier arrangement. The yellow CVL line ($578.2\,nm$) is used to pump the broad-band laser, and the green line ($510.6\,nm$) to pump the amplifier. At a pulse repetition rate of $10\,kHz$ the laser pulse duration is $18\,ns$. By means of a system of mirrors and lenses the laser beams are transported with an efficiency of 50 % to the apparatus located at a distance of $30\,m$. The gated ion counting system is triggered by the signal of a fast photodiode.

With this experimental setup one has two possible sources of background: (*i*) Rydberg atoms are produced in the charge exchange process and ionized together with the Rydberg atoms produced by laser excitation. (*ii*) Ions are directly produced in collisions with rest gas atoms. The Rydberg atoms formed in the charge-exchange cell are removed by filter 1, while the ions produced in the excitation region are extracted from the beam by filter 2. Thus only the Rydberg atoms formed in the excitation region and the ions produced in the region of the ionizer reach the detector and contribute to the background. The ionizer itself is constructed as an acceleration lens with eleven diaphragms at distances of $4\,mm$. The potential on these diaphragms increases gradually along the beam direction to a peak value of $7\,kV$ and then decreases sharply to zero. Here the maximum field strength on the axis is about $4 \cdot 10^5\,V/m$ which is sufficient to ionize Rydberg atoms of $n \geq 20$. This arrangement has two important advantages: *(i)* the ionization of laser excited Rydberg atoms is restricted to a volume of $1.5\,cm^3$, and *(ii)* the ions created

in this volume are accelerated after the ionization. The resulting energy difference of $3\,keV$ between these ions and the original beam can be exploited for a further discrimination against background.

This is demonstrated in Fig. 3 by an energy spectrum of the detected ions, obtained by varying the voltage of the deflector in front of the detector. The upper curve shows two distinct peaks corresponding to ions produced in collisions (left) and to ionized Rydberg atoms (right). This curve is obtained with the Rydberg atoms produced in the charge exchange process reaching the ionization region (Filter 1 at low potential). For the detection of laser excited Rydberg atoms, the deflector voltage is kept at the potential corresponding to the second peak. With an electrical field of $5 \cdot 10^5\,V/m$ at Filter 1, one obtains the lower curve of Fig. 3. The Rydberg peak is removed and only a small amount of background ions from collisions in the ionization region are deflected onto the detector. The background count rate is determined by the ultra high vacuum of $2 \cdot 10^{-9}\,mbar$ in the ionization region, which proves that the collisional formation of Rydberg atoms in the excitation region is small.

This background from collisional ionization corresponds roughly to the estimate:

$$N_{back} = \sigma_{coll} \cdot N_T \cdot I_P \cdot L_T \cdot \eta_L \approx 50/sec, \tag{5}$$

with a cross section for collisional ionization $\sigma_{coll} \approx 10^{-15}\,cm^2$ (Massey and Gilbody 1974), a density of target molecules $N_T = 6 \cdot 10^7/cm^3$, a current of projectile atoms $I_P = 3 \cdot 10^{10}/s$ (corresponding to a beam of $5\,nA$) and a length of the ionization region $L_t = 1cm$. The duty cycle η_L of the laser atom interaction is given by

$$\eta_L = \tau_{ia} \cdot \nu_{rep} = 3 \cdot 10^{-6}\,s \cdot 10^4\,s^{-1} = 3 \cdot 10^{-2}, \tag{6}$$

where τ_{ia} is the time of flight of the atoms through the interaction region and ν_{rep} the repetition rate of the copper vapour laser.

4 Results and evaluation of data

The apparatus was tested with measurements on the stable isotopes $^{168,170-174,176}Yb$. The ion count rate was recorded versus the Doppler tuning voltage at fixed frequencies of the dye lasers. An overall detection efficiency $\epsilon_{exp} = 1.5 \cdot 10^{-5}$ (22 ions/s

from a beam of $1.5 \cdot 10^6$ atoms/s at a signal-to-noise ratio of $S/N = 20$ and an integration time of $0.8\,s$ per channel) was measured on the weakest of the stable isotopes, ^{168}Yb which has the nuclear spin $I = 0$. The theoretical efficiency is given by

$$\epsilon_{theo} = \eta_L \cdot \epsilon_{pop} \cdot \epsilon_{exc} \cdot \epsilon_{ion} \cdot \epsilon_{trans}, \tag{7}$$

where η_L is the duty cycle of the laser, ϵ_{pop} the population of the $6s6p\,^3P_0$ state, ϵ_{ion} the ionization efficiency of the Rydberg atoms and ϵ_{trans} the beam transport efficiency. The overall excitation efficiency ϵ_{exc} can be estimated from saturation measurements in the two transitions and the considerations of section 2. The first excitation step is saturated with a laser power of $50\,mW$ (estimated value: $20\,mW$), whereas a saturation in the second step can not be achieved with the available power of $250\,mW$. With the approximate ratio of the saturation powers in the first and the second transition, $P^2_{SAT}/P^1_{SAT} = 50$ one obtains

$$\epsilon_{exc} = \frac{g_f}{\Sigma g_i} \times \epsilon_\tau \times 0.1 \approx 2.5\%, \tag{8}$$

where $\epsilon_\tau \approx 1/2$ allows for the decay of the intermediate state $6s7s\,^3S_1$ during the laser pulse. Reasonable values for the other efficiencies ($\eta_L = 3\%$, $\epsilon_{pop} = 5\%$, $\epsilon_{ion} = 80\%$, $\epsilon_{trans} = 70\%$) then give $\epsilon_{theo} = 2 \cdot 10^{-5}$ which is close to the experimental value. For isotopes with $I \neq 0$, the efficiency is reduced by about one order of magnitude, due to the splitting into a number of HFS sublevels.

The beams of radioactive ytterbium isotopes contain isobars of other rare earth elements with typical currents of more than $10^{10}\,atoms/s$. These give rise to a background of about $30\,ions/s$ on the detector (see Fig. 5), independent of the ytterbium fraction. Experiments on radioactive beams therefore require production rates of the order $10^6\,atoms/s$. This is nearly three orders of magnitude more than the minimum rate quoted by Sprouse et al. (1989) for fluorescence spectroscopy on the recoil products from heavy ion reactions in a cooled buffer gas cell. That technique, applied to the even isotopes, was limited mainly by the typical background of $1000/s$ (Sprouse et al. 1989), whereas in our case, apart from the duty cycle, the loss in the neutralization process and the inefficiency of the ionization reduce the sensitivity. The low efficiency of eq. (7) may be improved considerably by using a

pulsed ion source and an excitation scheme that starts from a more efficiently populated state. The gains will then proportionally reduce the minimum production rate required for spectroscopy.

Measurements were performed on the even isotopes in the sequence $^{156-166}Yb$ and the odd isotopes $^{157,159,175}Yb$. The even isotopes provide the connection between the isotope shifts in the transition $6s7s\,^3S_1 \rightarrow 6s21p\,^3P_2$ and the results of earlier measurements performed in the intercombination line $6s^2\,^1S_0 \rightarrow 6s6p\,^3P_1$.

The spectra that were recorded with a short time delay between the two laser pulses show a structure of several distinct peaks (Fig. 4). These can be explained by the mode structure of the first step dye laser. The resonance condition

$$\hbar(\omega_1^i + \omega_2) = E_{6s21p\,^3P_2} - E_{6s6p\,^3P_0} \tag{9}$$

is fulfilled for each mode (ω_1^i) of laser 1 with a correspondingly detuned frequency ω_2 of laser 2. The resulting transition probability to the upper state is a superposition of *(i)* two successive step by step transitions from the ground state to the Rydberg state (both lasers in resonance) and *(ii)* one two-photon transition (both lasers in or off resonance). If the first laser is detuned slightly from the resonance (i.e. if none of the modes is exactly in resonance with the first transition), the structure becomes asymmetric and the maximum ion count rate no longer appears at the center of the resonance.

To obtain a formula for the transition probability as a function of both laser frequencies, one has to solve the semi-classical system of differential equations for a three level system with two lasers (Letokhov et al. 1977):

$$\begin{aligned}
\dot{a}_{^3P_0} &= iV_1 e^{i\Omega_1 t} a_{^3S_1} \\
\dot{a}_{^3S_1} &= iV_1 e^{-i\Omega_1 t} a_{^3P_0} + iV_2 e^{i\Omega_2 t} a_{^3P_2} - \gamma a_{^3S_1} \\
\dot{a}_{^3P_2} &= iV_2 e^{-i\Omega_2 t} a_{^3S_1}
\end{aligned} \tag{10}$$

Here the $a_{^3P_0}$, $a_{^3S_1}$ and $a_{^3P_0}$ denote the population of the levels, Ω_i the detunings of the lasers from the resonance, V_i the amplitudes of the lasers and γ the decay from the intermediate state. The solution is obtained via a Laplace transformation:

$$|a_{^3P_2}|^2 = \sum_{j=1}^{N_m} \left| \frac{V_1 V_2}{(s_1^j - s_2^j)(s_2^j - s_3^j)(s_3^j - s_1^j)} \cdot \left[(s_3^j - s_2^j) e^{s_1^j t} + (s_1^j - s_3^j) e^{s_2^j t} + (s_2^j - s_1^j) e^{s_3^j t} \right] \right|^2 \tag{11}$$

where the s_i^j are the solutions of the characteristic equation

$$s^3+[\gamma+i(\Omega_1-\Omega_2)]\,s^2+[\Omega_1\Omega_2+V_1^2+V_2^2+i\gamma(\Omega_1-\Omega_2)]\,s+\gamma\Omega_1\Omega_2+i(V_2^2\Omega_1-V_1^2\Omega_2)\;=0 \tag{12}$$

and the summation refers to the contributions of different laser modes. In those formulas, the parameters γ, V_1, V_2, Ω_1 (the detuning of the nearest mode) and the mode distance have to be fitted to the experimental data. The fitting procedure yields the positions of the resonances within an uncertainty of $30\,MHz$ (typical uncertainties for narrow band fluorescence spectroscopy with low laser power are a few *MHz*). A fit of the lineshape from eq. (11) to the experimental resonance curve is given in Fig. 4 (solid line).

The large uncertainty in the evaluation of the line positions is likely to be due to the approximations in the model: *(i)* the time structure of both lasers is taken to be rectangular, which differs considerably from the experimental conditions (Belyaev et al. 1985) and *(ii)* the delay between the two lasers pulses is assumed to be zero. The time structure influences the spectral profile of the resonances, whereas the time delay determines the relative contributions of the two photon process and the step-by-step process to the total excitation probability. The step-by-step process is dominant if the delay between the two pulses is long enough. This is shown experimentally by a clear reduction of the mode structure when a time delay of $\Delta t \approx 8\,ns$ is introduced (Fig. 4). For the spectra recorded with such a delay, the center of the largest peak is a satisfactory approximation for the resonance position. These spectra yield the isotope shift with typical errors of $5\,MHz$ and are therefore taken for the evaluation of the final results (Table 1).

The electronic factor F^{576} for the isotope shift of the transition into the Rydberg state is obtained from a King plot (King 1984) connecting our measurements with those in the intercombination line $6s^2\,{}^1S_0 \rightarrow 6s6p\,{}^3P_1$, $\lambda = 555.6\,nm$ (Buchinger et al. 1982, Clark et al. 1979). The King plot yields $F^{576}/F^{556} = 0.119(2)$ with a perfect consistency of the measurements in both lines. Electronic factors F^{556} evaluated for the intercombination line range from $-10.9\,GHz/fm^2$ (Clark et al. 1979, King 1984) to $-12.1\,GHz/fm^2$ (Aufmuth et al. 1987). Here, we follow the tables of Heilig (1984) which contain the first complete list of $\delta <r^2>$ values based

on the measurements of Buchinger et al. (1982). In Table 1 the isotopes $^{157,159,175}Yb$ are incorporated into that list. Combined with other results (Clark et al. 1979, Sprouse et al. 1989) the values of $\delta <r^2>$ now cover the even isotopes $^{152-176}Yb$ and the odd isotopes $^{157-175}Yb$. We note, however, that a new evaluation of F^{556} can be based on the precision measurement of the hyperfine structure in the ytterbium ion (Blatt et al. 1983, Münch et al. 1987), yielding values of $\delta <r^2>$ that are generally about 9 % higher (Klempt et al. 1991).

The example of a measurement on the odd isotope ^{157}Yb is shown in Fig. 5. This spectrum was recorded with an integration time of 0.8 s per channel. The production rate was about $5 \cdot 10^7\, atoms/s$ with an isobaric contamination of $10^{10}\, atoms/s$. For this isotope and for ^{159}Yb, the yield was high enough for a measurement in both the transitions to the $^3P_2$ and $^3P_1$ Rydberg states, whereas for ^{175}Yb only the transition to $^3P_2$ was observed.

These HFS spectra of the odd isotopes yield additional information about nuclear spins and moments. The particular transition $6s7s\,^3S_1 \rightarrow 6s21p\,^3P_2$ involves states in which the HFS is determined only by the A-factors describing the magnetic interaction between s-electrons and the nucleus. The B-factors of the electric quadrupole interaction are expected to be zero unless there are admixtures of states with valence electrons of $l \neq 0$.

For a precise evaluation of the hyperfine constants A in the state $6s21p\,^3P_2$, the combined HFS pattern of the close-lying Rydberg states $^1P_1$ and $^3P_2$ has to be calculated. This requires a simultaneous diagonalization of the FS and HFS Hamiltonians for which explicit expressions can be found in Sobel'man (1972). In first order perturbation theory for degenerate states one obtains for the interaction matrix:

$$det\left(<k'|H_{FS} + H_{HFS}|k> - \delta_{kk'}\, W^{(1)}\right) = 0\,, \qquad (13)$$

where $W^{(1)}$ is the first order energy shift and the indices k,k' refer to the four (degenerate) fine structure states. The calculation of $W^{(1)}$ requires explicit knowledge of the wave functions of the states involved. Here, one can follow a procedure described by Rinneberg (1987), where the wave functions $|k>$ are taken as eigenfunctions of the fine structure Hamiltonian, $<k|H_{FS}|k'> = \delta_{k,k'} W_{FS}(k)$. The calculation of

the remaining matrix elements $<k|H_{HFS}|k'>$ can be performed in a basis of either LS-coupled (Rinneberg 1987) or jj-coupled (Lurio et al. 1962) wave functions. For the case of jj-coupling, the mixing coefficients c_1 and c_2 describe the contributions of the basic wavefunctions to the intermediately coupled states. The matrix elements of the two closest lying states, $^3P_2$ and $^1P_1$, are found to be (Lurio et al. 1962)

$$M^{33} = <^3P_2|H_{HFS}|^3P_2> = \frac{C}{2}\frac{a_{6s}}{4}, \tag{14}$$

$$M^{11} = <^1P_1|H_{HFS}|^1P_1> = \frac{C}{2}(\frac{c_1^2}{2} - \frac{c_2^2}{4})a_{6s}, \tag{15}$$

$$M^{13} = <^1P_1|H_{HFS}|^3P_2> = \frac{\sqrt{[4-(F-I)^2][(F+I+1)^2-4]}}{8}\, c_2\, a_{6s}, \tag{16}$$

where $C = F(F+1) - I(I+1) - J(J+1)$ and a_{6s} is the A-factor of the $6s$-electron which determines the HFS splitting in the Rydberg state. With these matrix elements, the first order energies of the levels write

$$W^{(1)} = \frac{1}{2}(M^{33} + M^{11} + \Delta E \pm \sqrt{4M^{31}\,M^{13} + (M^{33} - M^{11} - \Delta E)^2}), \tag{17}$$

where ΔE is the energy difference between the two states. The influence of the other two FS states, $^3P_1$ and $^3P_0$, can be neglected, because their distance in energy from the $^3P_2$ is $105\,GHz$ and $294\,GHz$, respectively (see Fig. 1).

For the $^3P_1$ state, the much weaker influence of the neighbouring FS levels can be calculated by second-order perturbation theory for the hyperfine structure (Lurio et al. 1962). The calculation of the perturbed energies $W^{(2)}$ again requires the off-diagonal elements $<^3P_1|H|^{3,1}P_J>$.

The complete HFS is now described by a modified hyperfine structure formula, including the parameters $A_{^3S_1}$, a_{6s} and the isotope shift IS:

$$\delta\nu = W^{(1,2)}(c_1, c_2, \Delta E, a_{6s}) - \frac{C_{^3S_1}}{2}A_{^3S_1} + IS \tag{18}$$

with

$$C = F(F+1) - I(I+1) - J(J+1) \tag{19}$$

where $W^{(1,2)}$ describes the energy eigenvalues of the combined FS and HFS interaction matrix. As explained above, these energies were calculated differently for $^3P_2$ and $^3P_1$. The A-factor of the $^3P_2$ Rydberg state is related to the single electron A-factor a_{6s} by $A_{6s21p} = a_{6s}/4$.

The analysis of the hyperfine structure in the $^3P_2$ state has been tested on the stable odd isotopes $^{171,173}Yb$, where similiar work was performed by Majewski (1985) and Rinneberg (1987). Table 2 gives a comparison between the different results. The agreement is quite satisfactory. Independent results for the mixing coefficient, $c_1 = 0.58(3)$, and the FS splitting $\Delta E = 6300(160)\,MHz$ were also obtained from the analysis of the spectra of ^{157}Yb and ^{175}Yb . A direct measurement of the FS splitting in the even isotope ^{168}Yb yields the much more precise value $\Delta E = 6250(25)\,MHz$.

The results for the A-factors of the $6s7s\,^3S_1$ state and a_{6s} from the analysis of the HFS in the Rydberg states are given in Table 1. The magnetic moments were calculated from the more accurate A_{6s7s} factors using as reference ^{171}Yb for which the magnetic moment $\mu = 0.49367(1)\mu_N$ is known from a precise optical pumping experiment (Olschewski 1972). The diamagnetic correction has been taken from Feiock and Johnson (1969). In analogy to the work on $^{159-169}Yb$ performed in the intercombination line (Neugart et al. 1983) an additional error of $\pm 0.007\mu_N$ has been assumed to acount for the HFS anomaly. The B-factors omitted in eq. (18) were found to be zero within the experimental errors. This was expected because only s-electrons determine the hyperfine structures. The p-electron contribution in the Rydberg state is negligible, because of the $1/n^3$ dependency of the hyperfine interaction (Gallagher 1988).

The spin $I = 7/2$ and the magnetic moment $\mu = -0.639(8)\,\mu_N$ suggest the assignment of an $f_{7/2}$ shell model wave function to the ground state of ^{157}Yb. A successive filling of the $f_{7/2}$ neutron shell is also observed for the neutron numbers $N = 83, 85, 87$ in a number of rare earth elements (Nd, Sm, Gd, Dy, and Er) around the proton subshell closure at $Z = 64$ (Neugart et al. 1983). It seems that this trend continues for Yb, whereas for the lighter elements Ba (Mueller et al. 1983) and Xe (Borchers et al. 1989) the $f_{7/2}$ state is only found for $N = 83$, next to the neutron shell closure. In the sequence of $N = 83$ to $N = 87$ the absolute values of the magnetic moments decrease from about $1\,\mu_N$ to $0.6\,\mu_N$ and the new value for ^{157}Yb fits well into this systematics. For ^{159}Yb, the analysis confirms the spin assignment $I = 5/2$ and the magnetic moment obtained from earlier measurements

in the intercombination line $6s^2\,{}^1S_0 \rightarrow 6s6p\,{}^3P_1$ (Neugart et al. 1983).

The measurement on ^{175}Yb gives the first precise value for the magnetic moment of this isotope with spin $I = 7/2$, $\mu = 0.766(8)\mu_N$. Earlier nuclear orientation work gave several inconsistent and much smaller magnetic moments (Benoit et al. 1974, Krane et al. 1972). The new value agrees rather well with the magnetic moment of the isotone ^{177}Hf and can be described by a rather pure Nilsson orbital [514 7/2].

5 Conclusion

The combination of collinear laser spectroscopy with resonance ionization detection has been shown to be a competitive technique for the investigation of unstable isotopes. It offers major advantages for beams with high isobaric contamination which require efficient background suppression.

The ionization efficiency is reduced mainly by the duty cycle of the copper vapour laser and the population of the metastable state. It could be increased by the use of a pulsed ion source (conventional or laser ion source) and with an excitation scheme that starts from a state which is more efficiently populated in the charge exchange process. Altogether a gain in sensitivity of 10 - 100 seems feasible, so that spectroscopy of 10^4 *atoms/sec* with a background contamination of 10^9 *atoms/sec* for an isotope with *I=0* is in reach.

This work has been funded by the German Federal Minister for Research and Technology (BMFT) under the contract number 06 MZ 188I.

References

Alkhazov G D, Barzakh A E, Denisov V P, Ivanov V S, Chubukov I Ya, Buyanov N B, Letokhov V S, Mishin V I, Sekatsky S K, Fedoseev V N, *Proc. 5th Int. Conf. on Nuclei far from Stability* (Towner I S, ed.) Vol. 164, AIP Conf. Proc. New York (1988) 115

Aseyev S A, Kudryavtsev Yu A, Letokhov V S, Petrunin V V, *Optics Letters* **16** (1991)

Aufmuth P, Heilig K, Steudel A, *Atomic Data and Nuclear Data Tables* **37** 455 (1987)

Aymar M, Champeau R, Delsart C, Robeaux O, *J. Phys. B* **17** 3645 (1984)

Balykin V I, Bekov G I, Letokhov V S, Mishin V I, *Usp. Fiz. Nauk* **132** 293 (1980) [English transl. *Sov. Phys. Usp.* **23** 651 (1980)]

Benoit A, Flouquet J, Sanchez J, *Phys. Rev. B* **9** 1092 (1974)

Bekov G I, Vidolova-Angelova E P, Letokhov V S, Mishin V I, *Opt. Spektrosk.***48** 435 (1980) [English transl. *Opt. Spectroscop. (USSR)* **48** 239 (1980)]

Belyaev V P, Zubov V V, Isaev A A, Lyabin N A, Sobolev Yu F, Chursin A D, *Kvantovaya Elektron. (Moscow)* 12 74 (1985) [English transl. *Sov. J. Quantum Electron.* **15** 40 (1985)]

Blatt R, Schnatz H, Werth G, *Z. Phys* **A312** 143 (1983)

Borchers W, Arnold E, Neu W, Neugart R, Wendt K, Ulm G, *Phys. Lett. B* **216** 7 (1989)

Breit G, Wills L, *Phys. Rev.* **44** 470 (1933)

Buchinger F, Mueller A C, Schinzler B, Wendt K, Ekström C, Klempt W, Neugart R, *Nucl. Instr. and Meth.* **202** 159 (1982)

Clark D L, Cage M E, Lewis D A, Greenlees G W, *Phys. Rev.* **A20** 239 (1979)

Ducas T W, Littmann M G, Freeman R R, Kleppner D, *Phys. Rev. Lett.* **35** 366 (1975)

Feiock F D, Johnson W R, *Phys. Rev.***187** 39 (1969)

Gallagher T, *Rep. Prog. Phys.* **51** 143 (1988)

Heilig K, *Hyperfine Interactions* **24** 349 (1985)

Kaufmann S L, *Optics Comm.***17** 309 (1976)

King W H, *Isotope Shifts in Atomic Spectra,* Plenum Press, New York (1984)

Klempt W, Neugart R, Wendt K, Ahmad S A, Ekström C, to be published

Krane K S, Olsen C E, Steyert W A, *Nucl. Phys.* **A197** 352 (1972)

Kudryavtsev Yu A, Letokhov V S, Appl.Phys. **B29**, 219 (1982)

Kudryavtsev Yu A, Petrunin V V, *Zh. Eksp. Teor. Fiz.* **94** 76 (1988) [English transl. Sov.Phys. JETP **67** 691 (1988)]

Lavi S, Bialolanker G, Amit M, Belker D, Erez G, Miron E, *Opt. Commun.* **60** 309 (1986)

Letokhov V S, Chebotayev V P, *Nonlinear Laser Spectroscopy* Springer, Berlin, Heidelberg, New York (1977)

Letokhov V S, Mishin V I, ISOLDE workshop, Zinal 1984 p.B8, unpublished

Lurio A, Mandel M, Novick R, *Phys. Rev.* **126** 1758 (1962)

Majewski U, Diplomarbeit, FU Berlin (1985);
private communication by Rinneberg H

Massey H S W, Gilbody H B, *Electronic and Ionic Impact Phenomena,* Vol. 4, Clarendon Press, Oxford (1974)

Münch A, Berkler M, Gerz Ch, Wilsdorf D, Werth G, *Phys. Rev.* **A35** 4147 (1987)

Mueller A C, Buchinger F, Klempt W, Otten E W, Neugart R, Ekström C, Heinemeier J, *Nucl. Phys. A* **403** 234 (1983)

Neugart R, Wendt K, Ahmad S A, Klempt W, Ekström C, *Hyperfine Interactions* **15/16** 181 (1983)

Neugart R, *Progress in Atomic Spectroscopy* (Beyer H J, Kleinpoppen H, ed.) Part D, Plenum Press, New York (1987), p. 75

Olschewski L, *Z. Phys.* **249** 205 (1972)

Otten E-W, *Treatise on Heavy Ion Physics* (Allan Bromley D A, ed.) Vol. 8, Plenum Press, New York (1988), p. 517

Ravn H, Allardyce B W, *Treatise on Heavy Ion Physics* (Bromley D A, ed.) Vol. 8, Plenum Press, New York (1988), p. 363

Rinneberg H, *Progress in Atomic Spectroscopy* (Beyer H J, Kleinpoppen H, ed.) Part D, Plenum Press, New York (1987), p. 157

Ross J, Murakawa K, *J. Phys. Soc. Jap.* **19** 249 (1964)

Ruster W, Ames F, Kluge H-J, Otten E-W, Rehklau D, Scheerer F, Herrmann G, Mühleck C, Riegel J, Rimke H, Sattelberger P, Trautmann N, *Nucl. Instr. and Meth.* **A281** 547 (1989)

Sobel'man I I *Introduction to the Theory of Atomic Spectra* Pergamon Press, Oxford, New York, Toronto, Sydney, Braunschweig (1972)

Sprouse G D, Das J, Lauritsen T, Schecker J, Berger A, Billowes J, Holbrow C H, Mahnke H E, Rolston S L, *Phys. Rev. Lett.* **63** 1463 (1989)

figure captions

Figure 1: Partial energy level diagram for *Yb I*, including the levels and transitions excited in this work. The inset gives the fine structure splitting of the Rydberg state.

Figure 2: Experimental setup for resonance ionization spectroscopy in collinear geometry.

Figure 3: Energy spectrum of ions produced without laser excitation. The peak on the left side corresponds to collisional ionization, the other to ionization of Rydberg atoms from the charge exchange process (upper curve). This peak is removed if the Rydberg atoms are ionized and deflected directly after the charge exchange cell (lower curve).

Figure 4: Spectra of ^{168}Yb, recorded with a delay of $3\,ns$ (left) and $8\,ns$ (right) between the two lasers. Details are given in the text.

Figure 5: Spectrum of ^{157}Yb. The frequency scale is given with respect to the reference isotope, ^{168}Yb.

Table 1: Isotope shifts and hyperfine structure constants in the transition $6s7s\,^3S_1 \longrightarrow 6s21p\,^3P_2$ of the investigated isotopes. The values for the magnetic moments have been evaluated from the A-factors of the $6s7s\,^3S_1$ state. $\delta <r^2>$ values have been calculated in accordance with the evaluation of Heilig (1985). Errors in brackets represent one standard deviation in units of the last significant figure. For the isotope shift and $\delta <r^2>$ they include voltage calibration errors of about $4 \cdot 10^{-3}$. The systematic error for the evaluation of $\delta <r^2>$ (about 10%) is not included. For details see text.

A	I	$IS^{168,A}\,[MHz]$	$\delta <r^2>\ [fm^2]$	$A_{6s7s}\,[MHz]$	$a_{6s}\,[MHz]$	$\mu\,[\mu_N]$
156	0	1528 (9)	-1.171 (24)	-	-	-
157	7/2	1425 (38)	-1.091 (36)	-1260 (6)	-2317 (24)	-0.639 (8)
		1397 (31)[1]		-1264 (4)	-2425 (190)	-0.639 (8)
158	0	1238 (8)	-0.955 (6)[3]	-	-	-
159	5/2	1101 (21)[1]	-0.846 (23)	-1021 (5)	-1976 (236)	-0.368 (8)
160	0	946 (7)	-0.732 (4)[3]	-	-	-
162	0	672 (7)	-0.516 (3)[3]	-	-	-
164	0	395 (8)	-0.314 (3)[3]	-	-	-
166	0	174 (9)	-0.140 (1)[3]	-	-	-
168	0	0	0	-	-	-
170	0	-152 (7)	0.117 (2)[3]	-	-	-
171	1/2	-200 (13)	0.157 (2)[3]	6837 (9)	12631 (84)	0.49367 (1)[2]
172	0	-277 (4)	0.228 (2)[3]	-	-	-
173	5/2	-313 (20)	0.266 (3)[3]	-1894 (8)	-3505 (20)	-0.684 (3)
174	0	-385 (12)	0.314 (3)[3]	-	-	-
175	7/2	-402 (14)	0.333 (13)	1519 (10)	2803 (19)	0.768 (8)
176	0	-482 (12)	0.397 (4)[3]	-	-	-

[1]: transition $6s7s\,^3S_1 \longrightarrow 6s21p\,^3P_1$

[2]: Olschewski (1972)

[3]: Heilig (1985) from experimental data of Buchinger et al. (1982)

Table 2: Values for the different parameters describing the hyperfine structure in the Rydberg state. For details see text.

	^{173}Yb		^{171}Yb	
	this work		this work	
c_1	0.58 (3)	0.54 (1)[1]	-	
$\Delta E\,[MHz]$	6170 (110)	4500 (3000)[2]	6260 (2900)	
$A_{6s7s}\,[MHz]$	-1894 (8)	-1892.2[3]	6837 (9)	6857.1[3]
$a_{6s}\,[MHz]$	-3500 (20)	-3497.2[4]	12631 (84)	12642.8[5]

[1]:calculated from Maejewski (1985)

[2]:Aymar et al. (1984)

[3]:Ross et al. (1964), no errror given

[4]:Münch et al. (1987), precision measurement with an errror of $3Hz$

[5]:Blatt et al. (1983), precision measurement with an errror of $1.4Hz$

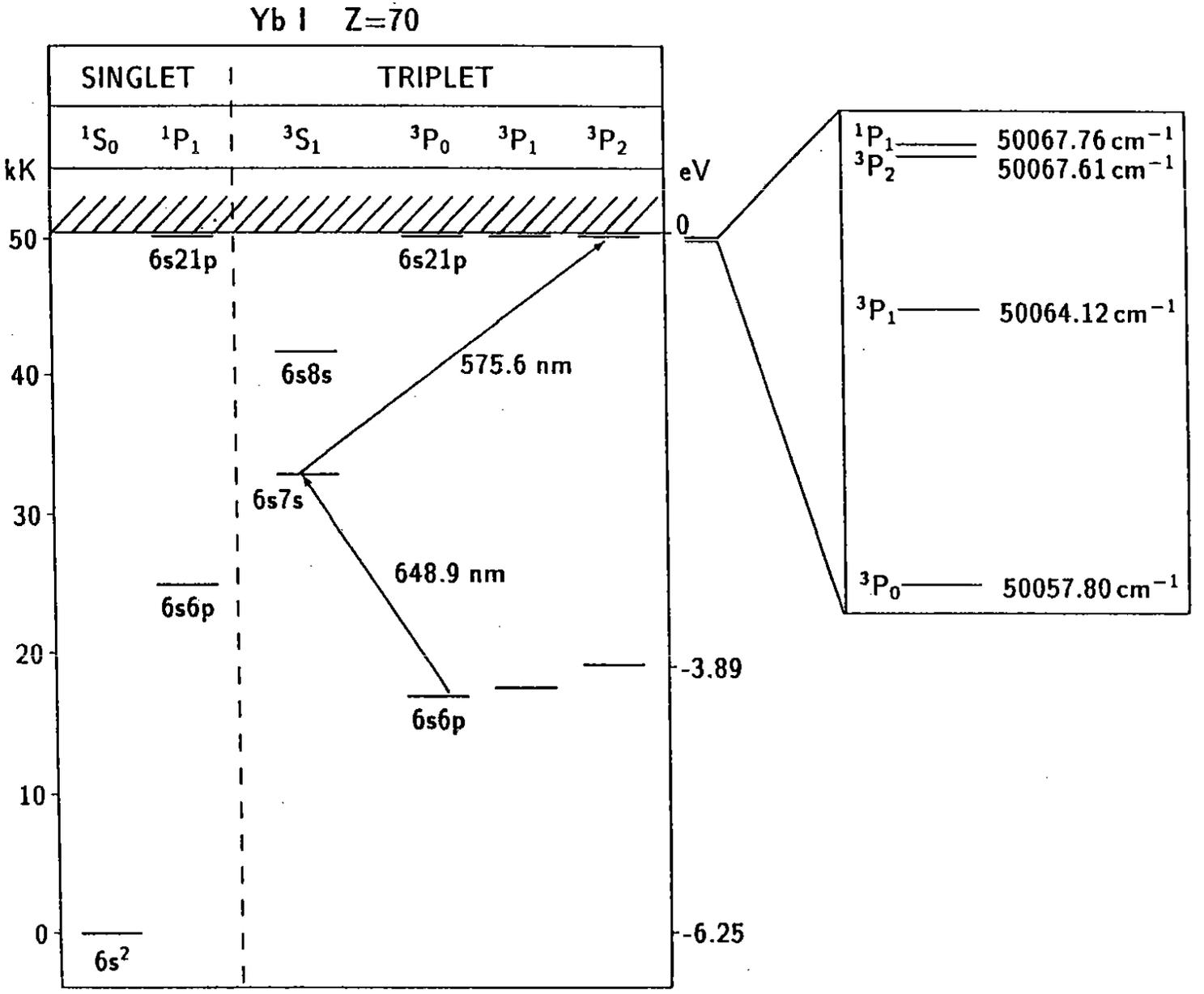
Yb I Z=70
SINGLET
TRIPLET
$^1S_0$
$^1P_1$
$^3S_1$
$^3P_0$
$^3P_1$
$^3P_2$
kK
eV
50
40
30
20
10
0
0
-3.89
-6.25
6s21p
6s21p
6s8s
6s7s
6s6p
6s6p
6s^2
575.6 nm
648.9 nm
$^1P_1$ 50067.76 cm^{-1}
$^3P_2$ 50067.61 cm^{-1}
$^3P_1$ 50064.12 cm^{-1}
$^3P_0$ 50057.80 cm^{-1}

Fig. 1

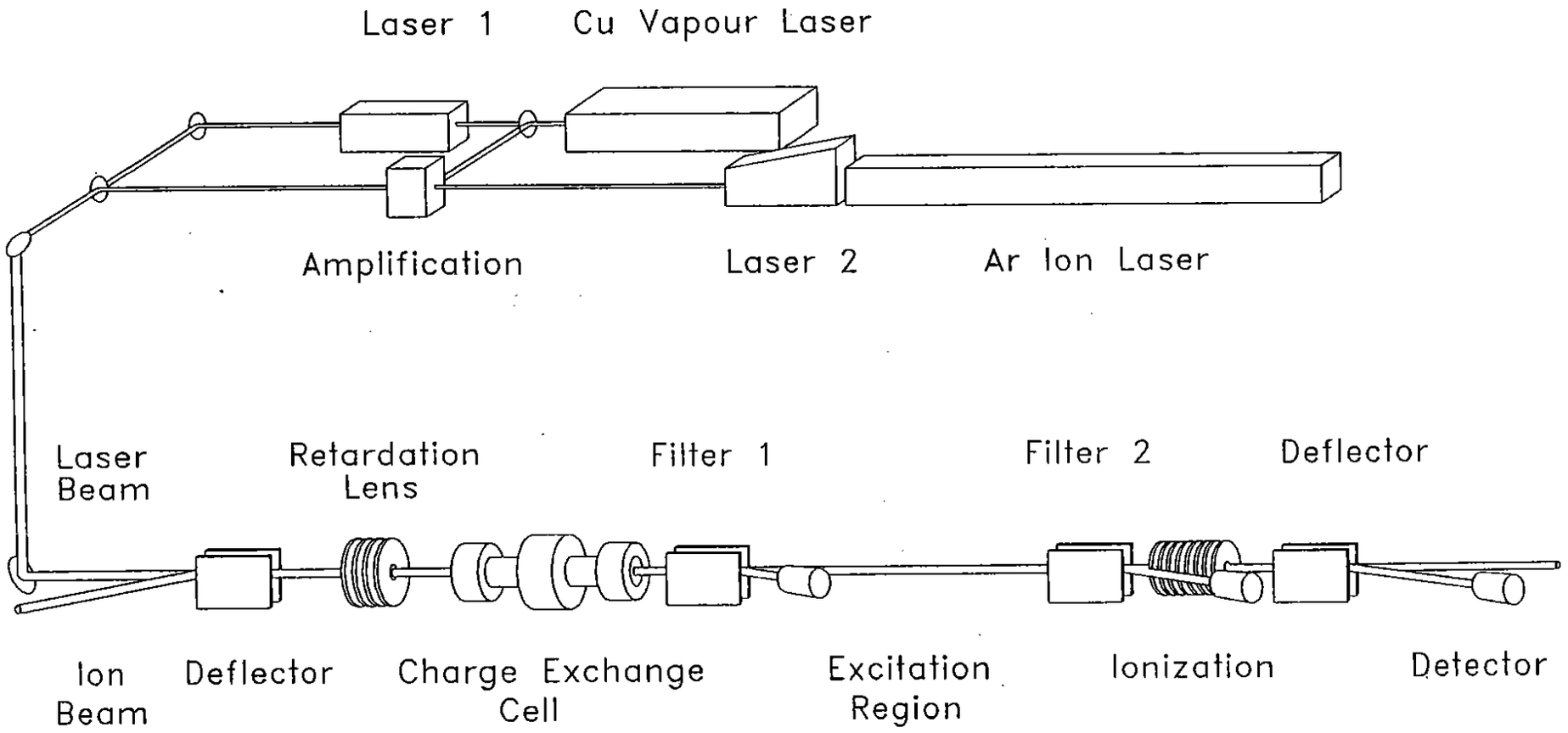
Laser 1
Cu Vapour Laser
Amplification
Laser 2
Ar Ion Laser
Laser Beam
Retardation Lens
Filter 1
Filter 2
Deflector
Ion Beam
Deflector
Charge Exchange Cell
Excitation Region
Ionization
Detector

Fig. 2

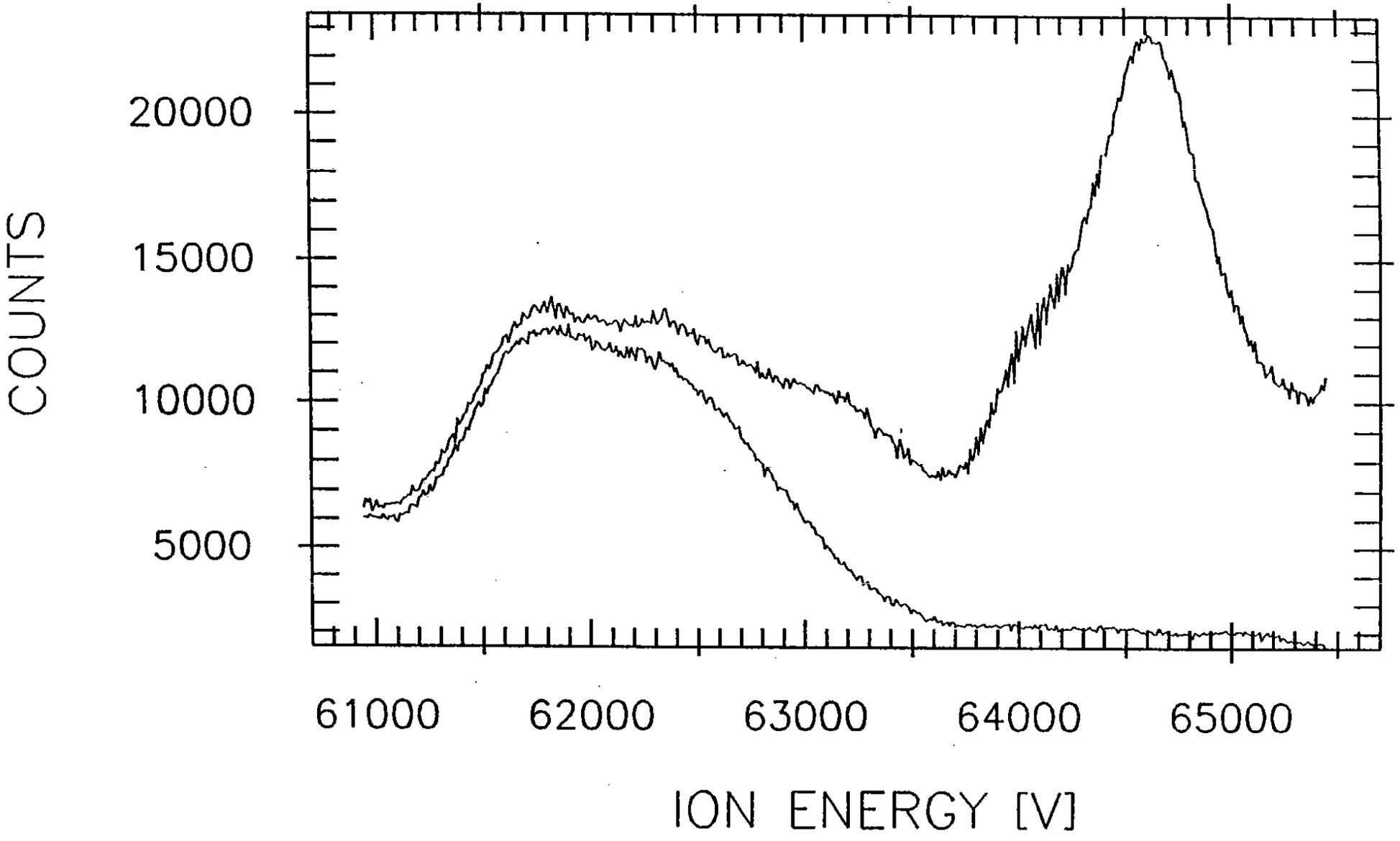
COUNTS
20000
15000
10000
5000
61000
62000
63000
64000
65000
ION ENERGY [V]

Fig. 3

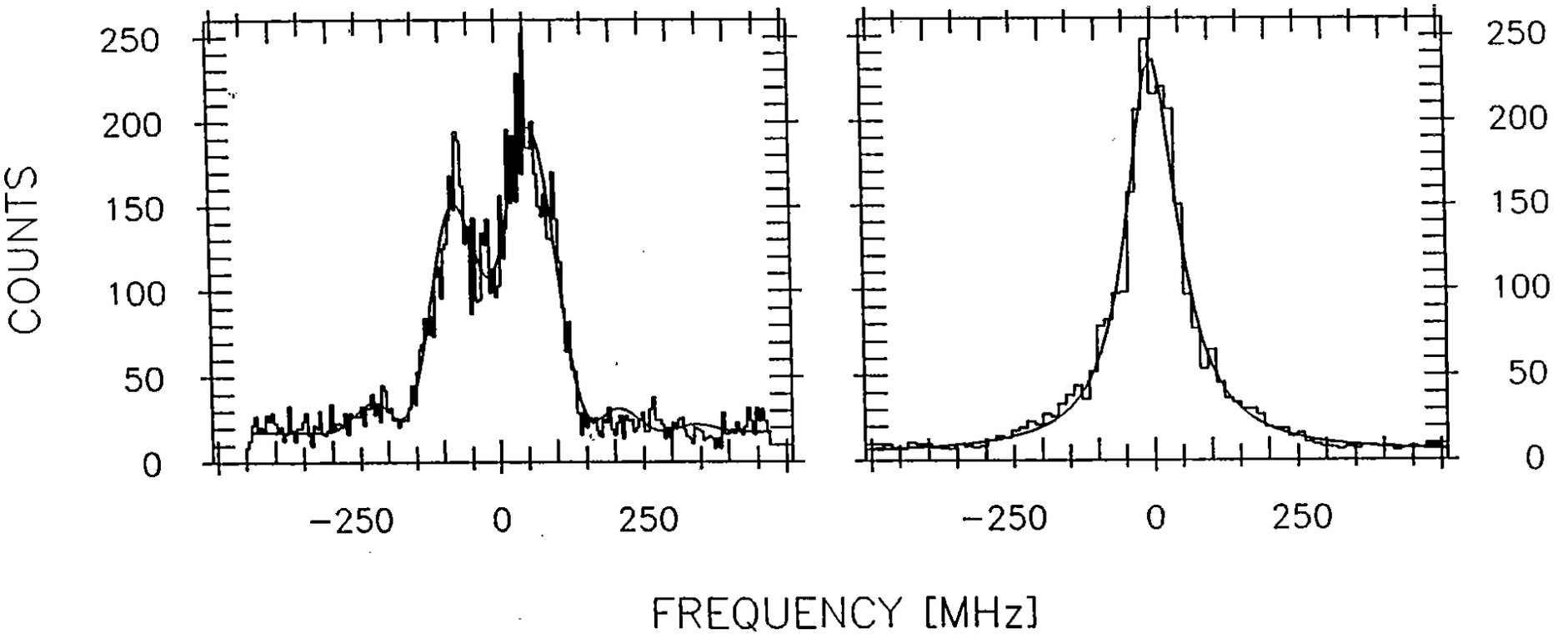

Fig. 4

Imprimé au CERN. Prix : 0.75 Fr.

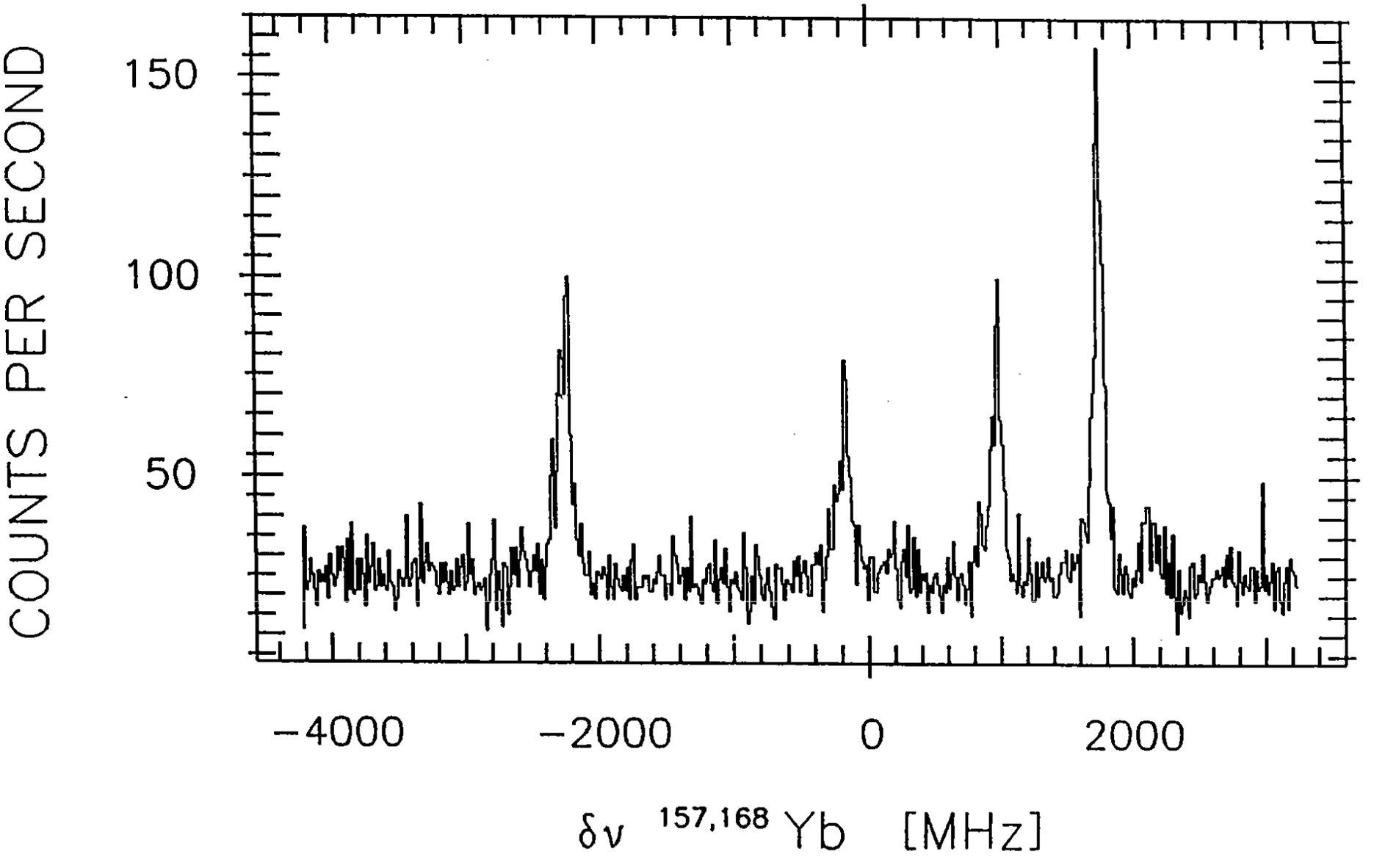

Fig. 5